Bulletin of Volcanology (2025) 87:4
https://doi.org/10.1007/s00445-024-01785-x

RESEARCH ARTICLE

Holocene onshore/offshore tephra correlation of Mt. Etna, Sicily

Antina Lippert[1,2] · Julie Christin Schindlbeck-Belo[2] · Thor H. Hansteen[2] · Paola Del Carlo[3] · Mirja Heinrich[2] · Boris Behncke[4] · Alessandro Bonforte[4] · Morelia Urlaub[1,2] · Henriette Kolling[1] · Rachel Barrett[1] · Felix Gross[1]

Received: 1 October 2024 / Accepted: 10 November 2024

Abstract
The volcanic history of Mt. Etna is mainly known from studies of subaerial deposits and stratigraphy. However, little is known about the offshore deposits, which can provide a more detailed insight into geological and sedimentological processes affecting the flanks of Mt. Etna. During RV Meteor Cruise M178, eight gravity cores were taken offshore across the continental margin east of the volcanic edifice to re-evaluate the volcanic history of pre-historic eruptions and mass wasting events in the area. In total, we investigated 87 marine tephra layers in order to build a marine tephrostratigraphic framework. Based on major element compositions of glass shards, sediment componentry, and petrographic characteristics, 27 layers were identified as primary pyroclastic flow and fall deposits, i.e., directly related to an explosive volcanic eruption. However, most of the remaining tephra layers are interpreted to represent deposits of secondary density currents and are not necessarily related to a volcanic eruption. The marine dataset is complemented by twelve onshore samples taken from major explosive eruptions. Applying geochemical fingerprinting of volcanic glass shard compositions, we correlated eleven marine tephra deposits to seven well-known Mt. Etna eruptions (FV, FF, FG, FL, FS, TV, and M1 eruptions) within the last 12 kyr, which provide valuable time markers in the marine sediment record. Furthermore, we correlated ten marine tephra layers between the marine cores (four individual eruptions) and identified another six primary layers in single cores. In total, we discovered 17 widespread volcanic events in the marine record, including four previously unknown eruptions between 10 and 7.7 ka, which indicate that Mt. Etna was more active than previously thought during this time period.

Keywords Mt. Etna · Holocene · Marine tephrostratigraphy · Onshore offshore tephra correlation

Introduction

Mt. Etna in Sicily (Italy) is the most active volcano in Europe. The volcanic activity can be classified in three types: (i) Strombolian activity or lava fountains at summit craters, (ii) flank eruptions, and, rarely, (iii) major caldera collapses and explosive eruptions that range from Subplinian to Plinian in size (Guest and Murray 1979; Salvi et al. 2006). Frequent eruptions have happened during the Holocene period, which have been studied on various timescales (Branca and Del Carlo 2004; Coltelli et al. 1998, 2000, 2005; Del Carlo et al. 2004; Branca et al. 2011). Historical records of volcanic activity on Mt. Etna go back to the Greek colonization period around 1300 BC. The first modern description of eruptions dates back to Thucydides in his "History of the Peloponnesian War," reporting the eruption of 425 BC, and mentioning another from 475 BC (Salvi et al. 2006). Onshore stratigraphic reconstruction of tephra deposits for the last 100 kyr are published by Coltelli et al. (2000) and Del Carlo et al. (2004). However, several major deposits still lack detailed geochemical analysis.

These stratigraphical approaches indicate an apparent time gap of ~ 3 kyr between the end of the Ellittico caldera-forming eruptions at about 15 ka, and the eruption that led to the deposition of the so-called M1 tephra layer at about

Editorial responsibility: W. W. Chadwick

✉ Antina Lippert
antina.lippert@gmx.de

[1] Institute of Geosciences, Kiel University, 24118 Kiel, Germany

[2] GEOMAR Helmholtz Centre for Ocean Research Kiel, 24148 Kiel, Germany

[3] Istituto Nazionale di Geofisica e Vulcanologia, Sezione di Pisa, Via C. Battisti 53, 56125 Pisa, Italy

[4] Istituto Nazionale di Geofisica e Vulcanologia, Sezione di Catania, Osservatorio Etneo, 95125 Catania, Italy

12 ka. After that, ten deposits were produced by Subplinian eruptions between 12 and 7.5 ka BP (Del Carlo et al. 2004). In the following years, between 7.5 ka BP and deposition of the TV layer (5340 ± 60 yr BP), the volcaniclastic succession is represented by 1–2-m-thick eolian deposits in which the record of explosive activity is scarce (Del Carlo et al. 2004).

Marine sediment records taken offshore Mt. Etna in the Ionian Sea can help to unravel and better understand the recent eruptive history of this active volcano. Furthermore, the correlation of marine tephra layers with their onshore equivalents provides important time markers in the marine sediments, helping to build an improved tephrostratigraphic framework of widespread volcanic eruptions.

Another important and basin-wide time marker in the investigated age range is the organic-rich sapropel S1 unit, which was deposited between 10 and 7.7 ka BP in the Mediterranean (Checa et al. 2020). Formation of sapropels is controlled by astronomical forcing, usually corresponding to phases of precession-induced insolation maxima (Rossignol-Strick 1985). These maxima provoke periods of humid climate in the Mediterranean region and produce organic-rich sedimentary layers. Ariztegui et al. (2000) states that the key factor that initiated the formation of S1 was increased discharge of freshwater into the Mediterranean, potentially fostering onshore erosion of volcanic deposits.

In this work, we present a detailed geochemical and petrographic analysis of marine tephra deposits of Mt. Etna collected from gravity cores recovered across the continental margin offshore the volcanic edifice. The geochemical analyses are combined with stratigraphic constraints of these tephras. We distinguish primary and secondary tephra deposits in the marine sediment records, and geochemically fingerprinted volcanic glass shards to establish correlations between onshore-offshore as well as offshore-offshore tephra deposits. The approach enables us to build a marine tephrostratigraphic framework for the investigated cores and extend knowledge of widespread volcanic eruptions of Mt. Etna over the last 12 kyr.

Geological setting

Overview

Mt. Etna has an altitude of 3,350 m, and is located on the east coast of Sicily within the complex structural geological setting of the western central Mediterranean (Doglioni et al. 2001). Volcanic activity continues to build up the edifice onshore, but the edifice extends significantly onto the adjacent submarine continental margin (Chiocci et al. 2011; Gross et al. 2016).

The onshore stratovolcano is built up by several volcanic edifices and calderas. At an altitude of 2800 to 2900 m, Mt. Etna volcano is truncated by the Ellittico and Cratere del Piano interlocking calderas. The Ellittico caldera formed at the end of the Ellittico period of volcanic activity, approximately at 15 ka (Coltelli et al. 2000). The caldera rim of Ellittico outcrops at Punta Lucia and Pizzi Deneri on the northern flank. On the southern flank, the caldera rim is buried by the products of Mongibello volcano (Fig. 1A), but is recognizable by the sudden change in steepness on the western upper flank of the volcano. The Cratere del Piano is a 2 km wide caldera that formed during the eruption of 122 BC (Coltelli et al. 1998). Inside these two calderas, the Mongibello volcano forms a large summit cone in which four summit craters have evolved during the last century: the Northeast-Crater (NEC, 1911), Voragine (VOR, 1945), Bocca Nuova (BN, 1968), and Southeast Crater (SEC, 1971) (Behncke et al. 2014) (Fig. 1).

Roughly at 9 ka, the Valle del Bove (VdB) opened through catastrophic failure of the Ellittico volcano (Malaguti et al. 2023). This event was followed by a rapid enlargement of the newly formed VdB through landslides and fluvial reworking (Calvari et al. 1996).

Formation of the central volcanic complex, after the first effusive activity, started around 110 ka with the eruption of alkaline magmas (Branca et al. 2011). Explosive activity of Mt. Etna has been subdivided into five onshore tephrostratigraphic units from A to E (Coltelli et al. 2000). The oldest Unit A (100 ka) is characterized by basaltic Strombolian eruptions. Unit B (80–100 ka) is mainly composed of products of benmoreitic Plinian eruptions, marking the end of the Trifoglietto volcanic phase. Unit C is called the post-Trifoglietto and Ellittico phase (16–80 ka) and is characterized by Strombolian to Subplinian eruptions with basaltic to mugearitic compositions (Coltelli et al. 2000).

Deposits of Unit D were erupted between 19 and 17 ka (Albert et al. 2013; Del Carlo et al. 2020). This short period is associated with the end of the Ellittico volcano activity, which was characterized by 5 Plinian eruptions of benmoreitic to trachytic composition (Coltelli et al. 2000; Del Carlo et al. 2017) (Table 1).

Unit E is the most recent unit. Its deposition started at 12 ka and continues until today. Its deposits cover the entire Mt. Etna edifice and comprise several tephra marker beds. This unit is the most important for this study covering the Holocene, and we therefore describe it in greater detail in the following section.

Stratigraphy of Unit E (onshore)

The lowermost tephra layer, M1 (12,240 ± 60 yr BP) (Coltelli et al. 2000), is a lithic-rich scoria alternating with fine ash beds that contain accretionary lapilli (Del Carlo et al. 2004) (Fig. 2).

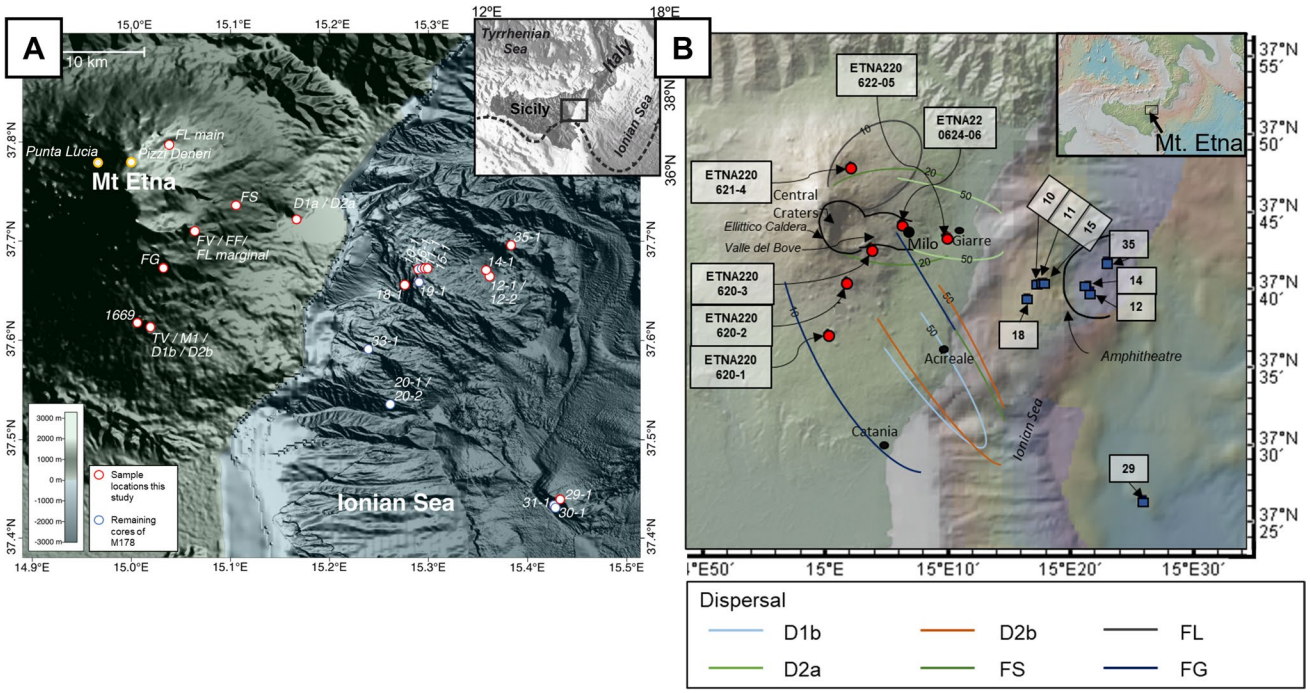

Fig. 1 **A** Schematic map of Mt. Etna showing all onshore and offshore sampling locations as well as morphological features offshore; **B** map of Mt. Etna (from: http://www.geomapapp.org) region showing the outcrops and the isopachs of previously identified eruptions (Coltelli et al. 2000). Colored lines represent isopachs for eruptions D1b, D2a, D2b, FS, FL, and FG (Coltelli et al. 2000). Numbers represent the core numbers of expedition M178

Table 1 Short sample descriptions with sites, age, dispersal, lithology, and composition. After Coltelli et al. (2000), Del Carlo et al. (2004) and Mulas et al. (2016)

Label	Eruption	Coordinates	Age (yr)	Dispersal	Lithology	Glass composition this study
Etna22-1	1669 Eruption	N 37° 37.056660 E 15° 0.387840	353	NE	Scoria lapilli	Hawaiite-Mugearite
Etna22-2	FG (122 BC)	N 37° 40.381020 E 15° 1.907400	2,180 ± 60 (122 BC)	SE	Scoria lapilli and tuff beds	Mugearite-Phonotephrite-Benmoreite
Etna22-3	FV	N 37° 42.593700 E 15° 3.846120	1,260 ± 60	ESE	Scoria lapilli	Mugearite-Phonotephrite
	FF		44 BC	NNE	Scoria lapilli	Mugearite-Phonotephrite
	FL (marginal area)					
Etna22-4	FL (main area)	N 37° 47.800560 E 15° 2.253720	3,150 ± 60	NE	Scoria lapilli and tuff beds	Tephriphonolite-Benmoreite-Phonotephrite-Mugearite
Etna22-5	D2a	N 37° 43.303560 E 15° 10.020060	15,050 ± 70	E	Pumice	Trachite
	D1a		15,420 ± 60	E	Pumice	Trachite
Etna22-6	FS	N 37° 44.174880 E 15° 6.348180	3,930 ± 60	E	Scoria lapilli	Picrite Basalt
	TV	INGV-OE repository	5,340 ± 60	Circular	Lithic-rich tuff	Phonotephrite-Mugearite
	M1	INGV-OE repository	12,240 ± 70	E	Scoria lapilli and tuff beds	Mugearite
	D2b	INGV-OE repository				
	D1b	INGV-OE repository				

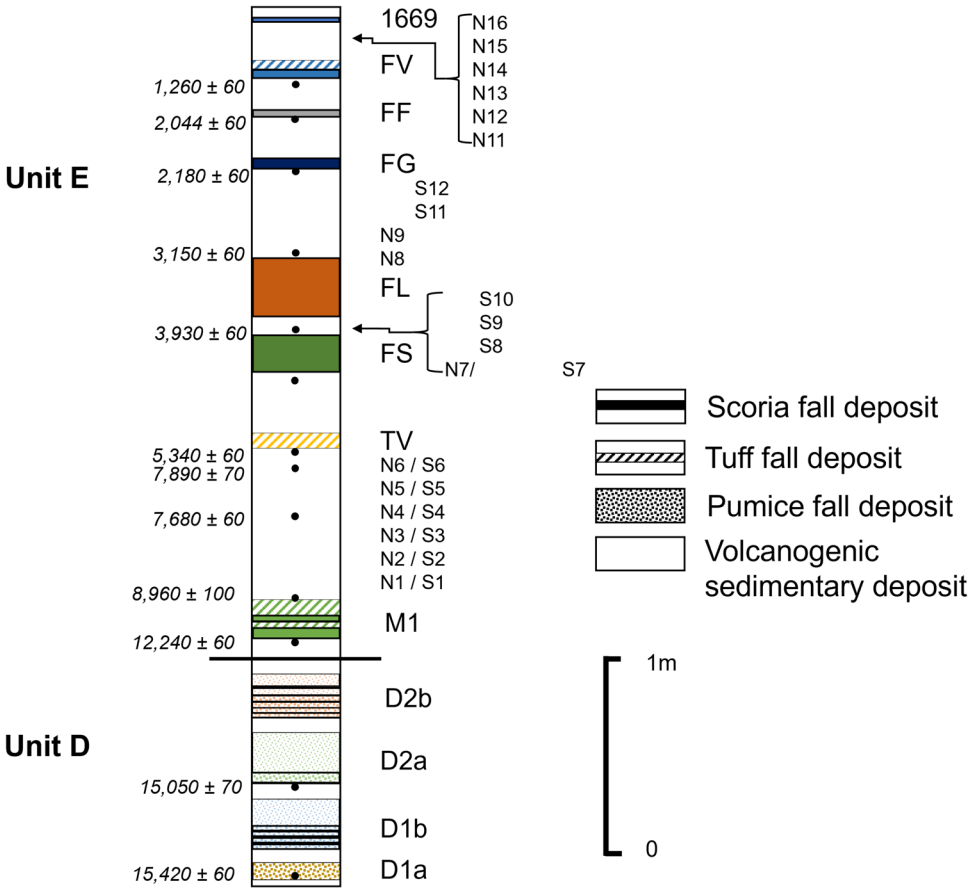

Fig. 2 Schematic stratigraphic profile of Mt. Etna pyroclastic deposits of Unit D and E, modified after Del Carlo et al. (2004) and references therein. Age for layer FS is from Malaguti et al. (2023). Numbers on the left side are the respective ages in "yr BP." Black dots mark the position of samples used for ^{14}C-dating.The colors associated with the tephras in this figure are used throughout the manuscript

There are at least twelve tephra deposits following M1 between 12 and 5.3 kyr BP, called S1-S6 (S = South) and N1-N6 (N = North) (Fig. 2). Tephra layers S1, S2, S3, S4, S6, N1, N2, N3, and N4 are lapilli fall deposits and are made of oxidized gray to reddish scoria, often including oxidized lithic clasts (Del Carlo et al. 2004). Some lapilli layers are interbedded with vesiculated or laminated tuff beds. N5 and S5 are thick varicolored tuff layers with accretionary lapilli; N5 has an age of 7980 ± 60 yr BP and can be traced in several sections in the NE sector. A pumice fall layer (N6) was erupted at around 7.6 kyr BP. This Subplinian eruption is widely dispersed in the NE and SE sectors of Mt. Etna (Del Carlo et al. 2004).

In the Milo area, a complex succession of debris flow deposits outcrops and was named the Milo lahar by Romano (1982). The succession begins with a debris-avalanche deposit related to the opening of VdB (Calvari et al. 1998) and continues upward with a set of lahar-type deposits.

The phreatomagmatic TV layer, which is generally a gray to pink varicolored tuff, was deposited at 5340 ± 60 yr BP (Coltelli et al. 2000) (Fig. 2).

Above the TV layer lies a scoria layer associated with the Subplinian FS eruption (3930 ± 60 yr BP); a picritic basalt with a high olivine content (Coltelli et al. 2000, 2005) (Fig. 2). According to Coltelli et al. (2005), the material was dispersed towards the east (Fig. 1B, Table 1). The frequency of the explosive eruptions at Mt. Etna doubled after the FS eruption (Del Carlo et al. 2004).

The FL scoria layer (3150 ± 60 yr BP) is characterized in the medial dispersal area by a high content of large plagioclase crystals. The lithics are massive and altered. In the proximal dispersal area, the FL layer is represented by a whitish, fine tuff layer. Generally, this bed is interpreted as having been produced by a complex phreatomagmatic eruption of vulcanian intensity (Del Carlo et al. 2004) (Fig. 2).

A major basaltic Plinian eruption occurred in 122 BCE (paleosol age below the tephra is dated to 2180 ± 60 yr BP) and produced the widely dispersed FG tephra bed (Coltelli et al. 1998, Bisson and Del Carlo 2013). A significant part of the deposit covered Catania and has been identified up to 400 km southeast in cores on the Malta Rise in the Mediterranean Sea (Coltelli et al. 1998; Micallef et al. 2016) (Figs. 1B and 2, Table 1).

The FF tephra (2044 ± 60 yr BP) deposit was produced by a Subplinian eruption (Del Carlo et al. 2004).

Immediately on top of the FF layer, the highly vesicular hawaiitic FV scoria layer (1260 ± 60 yr BP) is deposited (Coltelli et al. 2000) (Table 1).

The 1669 eruption was the most destructive flank eruption of Mt. Etna in recent historical times. Generally, the pyroclastic fall units were deposited around Monti Rossi, with only the fine material being dispersed towards the NE (Mulas et al. 2016) (Table 1). The scoria is highly vesicular with visible clinopyroxenes. The 1669 event can be considered as an archetype example of the most hazardous eruption to be expected on the densely populated flank of Mt. Etna (Mulas et al. 2016).

Methods

Sampling

During a field campaign in June 2022, six outcrops (Etna220620-1 to Etna220624-6) were logged, and twelve major tephra marker horizons of Unit D and E (Fig. 1, Table 1) were sampled for correlation purposes. Samples were taken as bulk samples (ca. 1–2 kg) within the main body of the respective deposit. We were not able to take samples from D1b and D2b due to recent development blocking access, but samples were provided by the rock repository of INGV-OE.

Marine sediment layers (87 samples) were taken from eight gravity cores (GC) recovered during *RV Meteor* expedition M178 east of Mt. Etna in 2021 (Gross et al. 2021) (Fig. 1, supplementary table E). The core locations were selected after analyzing the hull-mounted parametric Sediment Echosounder Teledyne Atlas Parasound P70 profiles and multibeam bathymetric data of the area. All cores, except M178-29, which is the most distal from the coast, lie on structural highs or lows of the structural amphitheater offshore Mt. Etna (Fig. 1). All cores were visually described in terms of their sediment lithology, including colors according to the MUNSELL soil color chart and sedimentary structures. Descriptions and photographs of the sediment core segments are presented in the appendix of the M178 cruise report (Gross et al. 2021) and in the supplement I. Discrete tephra layers were sampled on board and onshore from the working-halves of the cores.

Analysis

Electron microprobe analyses

All 87 marine and 14 terrestrial samples were cleaned, sieved into different fractions, and analyzed in the laboratories of GEOMAR Helmholtz Center for Ocean Research, Kiel, for geochemical composition. For the terrestrial samples, we selected the most fresh and unaltered juvenile clasts before crushing and sieving. Glass shards were analyzed for their major element composition using an Electron Microprobe (EMP). EMP analyses were conducted on epoxy-embedded samples on the > 63–125 µm and > 125–250 µm fractions using a JEOL JXA 8200 wavelength dispersive EMP. We used a beam diameter of 10 µm and a beam current of 6 nA with an accelerating voltage of 15 kV following the methods described in Kutterolf et al. (2011). The full list of standards used for calibration is provided in the supplementary table H.

Natural and synthetic glasses and minerals were used as standards for calibration. Accuracy was monitored by standard measurements on Lipari obsidian (rhyolite) (Hunt and Hill 2001) and Smithsonian basaltic standard VGA (reference A-99 Makaopuhi Lava Lake). If available, 20 individual glass shards were measured per sample. After every 60 measurements, four measurements on standards (always two for the Lipari standard, two for the VGA standard) followed to verify the instrument stability during each analytical session. Standard deviation is 0.5% for major elements, and all standard measurements are provided in supplementary table D. All analyses were normalized to 100 wt% anhydrous composition to avoid the effects of variable post-depositional hydration and to enable valid comparison with tephra deposits from various environments (Allan et al. 2008; Pearce et al. 2008, 2014a,b; Lowe et al. 2011). In total, we analyzed 1479 individual glass shards. However, we deleted analyses with a total < 95 wt% and accidental shots on minerals to finally acquire 1022 good quality measurements. Geochemical analyses of the two grain size fractions yielded indistinguishable results. All analyses that passed the quality check are provided in the supplementary tables A and C.

^{14}C dating

We performed ^{14}C dating on a mussel sampled from M178-14, 330 cm, which yielded an age of 5775 ± 35 yr BP, corresponding to a calibrated age of 6487–6666 yr cal BP (calibrated with OxCal v4.4; Bronk Ramsey 2021; IntCal20 Reimer et al. 2020). The sample was processed at the Leibniz Laboratory for Age Determination and Isotope Research at Kiel University and analyzed with a HVE 3MV Tandetron 4130 accelerator mass-spectrometer (supplementary table F).

Point counting

Point counting was conducted following the procedures described in Menke et al. (2018) for a semiquantitative estimation of pyroclast abundance applied to BSE (backscattered electron) images on 29 selected samples. We used a regular net with 961 points on top of the respective BSE pictures of each analyzed sample to create a grid, and distinguished between volcanic glass, minerals, and biogenic

material. A detailed overview of the results is provided in the supplementary table B.

Correlation techniques

We applied the "geochemical fingerprinting" technique on glass shards to correlate between onshore/offshore or offshore/offshore tephra layers (Derkachev et al. 2020; Kutterolf et al. 2008, 2016; Lowe et al. 2011, 2017; Schindlbeck et al. 2016, 2018a, b; Menke et al. 2018). To obtain a reliable outcome, the method was combined with macroscopical and microscopical observations as well as stratigraphic criteria. We used several bivariate plots of the major element oxide concentrations and ratios of volcanic glass shards to correlate the tephra layers across the different samples. We drew correlation fields for the terrestrial tephra layers based on our new dataset of glass shard compositions.

Results

Onshore outcrop descriptions

Tephra samples from well-known marker horizons from Unit E were sampled in five outcrops or provided by the INGV-OE repository in Nicolosi (Table 1). The deposits of the M1 and TV eruptions are no longer exposed in the field because of vegetation overgrowth or anthropogenic development.

Outcrop Etna220620-1 represents a 3–4-m-thick exposure of the 1669 eruption deposit located at the Monti Rossi (see Figs. 1B and 3b). This deposit displays horizontal stratification characterized by fine (dark ash) and coarse (black scoria lapilli to bombs) materials in alternating layers (Fig. 3b). The scoria lapilli are highly vesicular, hosting clinopyroxene phenocrysts that are visible with the naked eye.

Outcrop Etna220620-2 (Fig. 1B, supplementary Fig. 1a) at Monte Salto del Cane is a key location for the 122 BC eruption (FG tephra layer). The 60-cm-thick scoria fall deposit is stratified and partially eroded at its upper surface. FG begins with a several centimeter-thick layer of black coarse ash at the base, followed by a bed of scoria lapilli and a minor amount of lava lithic clasts. These lapilli exhibit hues ranging from brown to dark gray, characterized by micro-vesicular texture and abundant crystals, and prominently featuring large plagioclase crystals.

At outcrop Etna220620-3 (Fig. 1B, supplementary Fig. 1b), four discrete tephra layers of the FL, FG, FF, and FV eruptions (from bottom to top) are visible and separated by thin soil layers. The outcrop has an average height of 2 m. The FL deposit in this outcrop is only visible close to the limit of the actual distribution of this unit. Here, the FL tephra is represented by a whitish layer of fine ash and has a thickness of 5–7 cm. The FG tephra layer is up to 20 cm thick, but is not well preserved at this site. The FF tephra consists of coarse ash and a centimeter thick scoria lapilli bed and is 5–6 cm thick in outcrop. In this outcrop, the FV scoria lapilli layer was not well preserved with only a few centimeters of material.

At outcrop Etna220621-4 (Fig. 1B), the poorly sorted deposits of the FL eruption can be found (30 cm thickness; Fig. 3c). The scoria lapilli are glassy and poorly vesicular and characterized by a high abundance of giant plagioclase crystals. The lithic lava fragments are massive and heavily altered.

At outcrop Etna220622-5 (Fig. 1B), the deposits from the D1a (supplementary Fig. 1c) and D2a (supplementary Fig. 1d) eruptions are exposed. The D1a deposit is a normal graded, slightly stratified pumice lapilli layer with a thickness of 38 cm. The larger lapilli within this layer typically range from 5 to 6 cm, with a reduction in grain sizes towards the upper portion. Additionally, weathered, reddish lava fragments are present in the deposit. The pumice lapilli exhibit elongated vesicles. Notably, the D2a layer in this location is solely represented by a few lenses of pumice lapilli, approximately 15 cm thick, positioned atop the D1a layer.

Outcrop Etna220624-6 is located in an old quarry close to Fornazzo village (Figs. 1B and 3a). The deposits of the FS eruption are exposed and up to 70 cm thick. This layer displays stratification resulting from alternating beds of fine and coarse grains associated with colors ranging from reddish to violet. The entirety of the deposit exhibits slight inverse grading and generally lacks sorting. Notably, at a depth of 40 cm from the base, there is a gray 4-cm-thick ash-rich layer. The scoria lapilli of FS layer contain mm-sized olivine crystals.

Marine tephra inventory

Sediments recovered during the M178 cruise consist mainly of silty clays of olive to grayish brown color (Fig. 3d, e, h). Sparse carbonate shells, mostly molluscs and scaphopods, were found. The eight investigated cores contain a total of 87 ash/lapilli-bearing horizons (Fig. 3e, f, h) with different amounts of glass (< 5 up to 65 vol%) (Fig. 3g, i, j). The medium to poorly vesicular glass shards are mostly blocky with predominantly round and elliptical bubbles. Glass shards are transparent and brownish and microlite rich. The main mineral assemblages comprise plagioclase, clinopyroxene, and sometimes olivine. The tephra layers are intercalated within hemipelagic sediment and range from 0.1 to 6 cm in thickness (Fig. 3d–f, h). Most cores from the basins show dark brown to gray-brown organic-rich layers, which have been regularly observed in marine sediment sections in the eastern Mediterranean and are called sapropels (e.g., Grimm et al. 2015; Emeis et al. 1996; Capotondi et al.

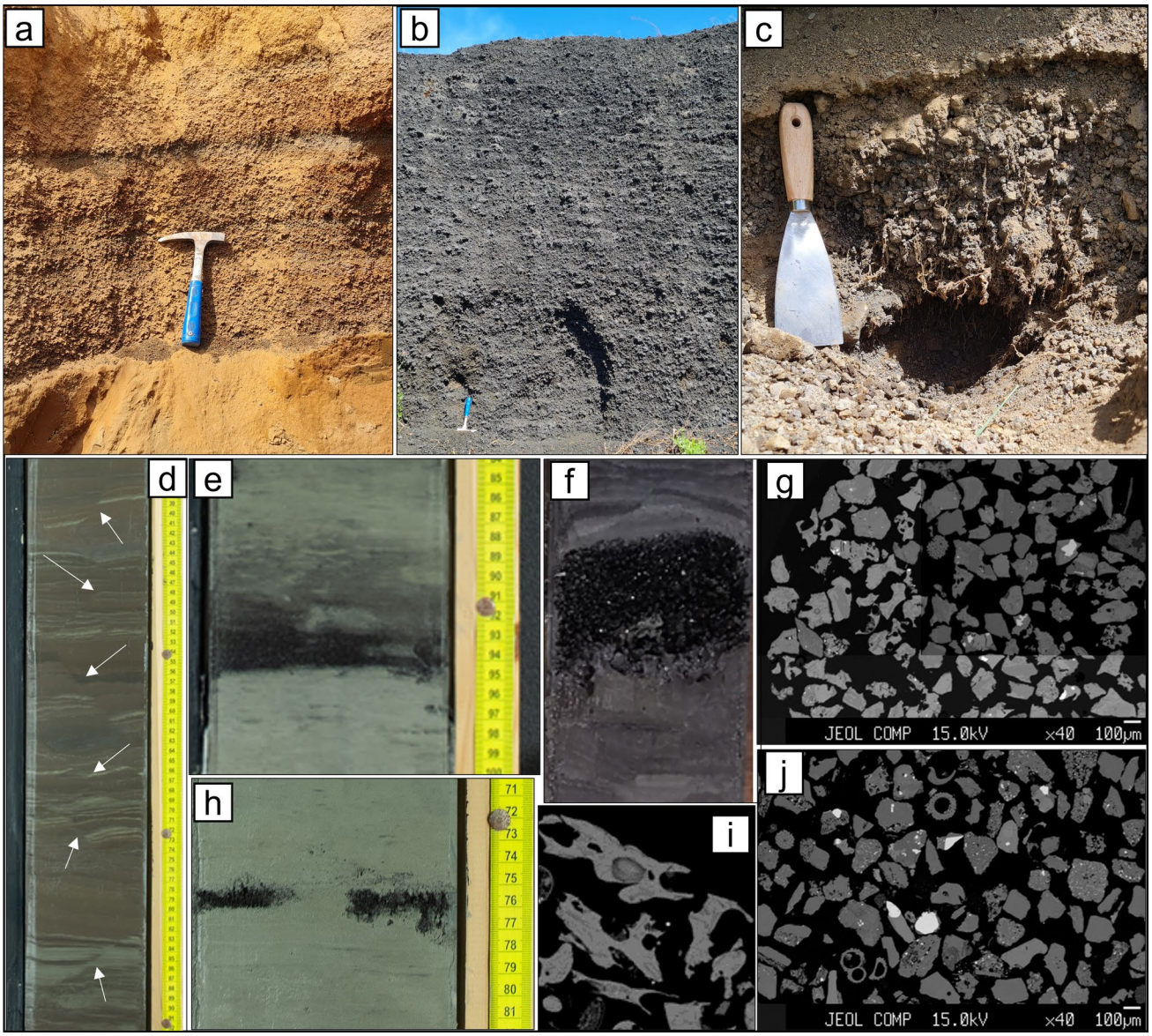

Fig. 3 Selection of photographs of deposit outcrops and marine cores. **a** Outcrop Etna220624-6 of the FS marker bed in an old quarry near Fornazzo. **b** Outcrop Etna220620-1 of the 1669 eruption near the Monti Rossi. **c** Outcrop Etna220621-4, detail of the FL marker bed in the main dispersal area of the eruption products. **d** Segment of the M178-15 core containing the sapropel layer showing fractures and faults (marked with white arrows). **e** Primary marine tephra M178-18, 189 cm, with a sharp basal contact, which was correlated with the FG marker bed. **f** Primary marine tephra M178-35, 414 cm showing a sharp basal contact. This layer is associated with eruption MB4. **g** An exemplary BSE picture of a primary marine tephra layer (M178-35, 538 cm). **h** Primary marine tephra layer of the M178-11, 275 cm sample, correlated to the FS layer. **i** BSE picture of glass shards measured (M178-35, 505 cm) with the EMP (electron microprobe). **j** Exemplary BSE picture of a secondary marine tephra layer (M178-35, 574 cm)

2011; Checa et al. 2020) (Fig. 3d). As these horizons occur in most cores within the uppermost 4 m, they are interpreted to correspond to the youngest sapropel S1 (Gross et al. 2021), which is dated to the interval between 10 and 7.7 kyr BP (Checa et al. 2020). This is supported by the ^{14}C age obtained above the sapropel in core M178-14. The thickness of the sapropel within the cores is up to 3.5 m, although it is not possible to know the complete thickness of the sapropel in most cores, as some terminate within the sapropel layer (Fig. 3d).

Sediment cores recovered from structural highs, such as the headwall in the amphitheater (M178-10, −11, −15) or ridges outside the amphitheater (M178-18, −29, −35), commonly contain sections with tectonically overprinted sediments. The recovered cores also show micro-fractures, including normal faults with vertical displacements

(Fig. 3d). Gravity cores retrieved from morphological depressions, such as cores M178-12 and −14 in the amphitheater, regularly exhibit mass transport deposits. These deposits can range from a few centimeters of fine-grained layers to meter-thick reworked sediment bodies consisting of coarse lapilli, sandy tephra, and shell debris.

The point counting results indicate an average glass shard abundance of approximately 26% by volume, accompanied by a low proportion of biogenic material (2.5% by volume) and minerals (65% by volume). This average was observed in most samples of cores from morphological highs. Lower amounts of glass shards, sometimes with a higher proportion of organic material (8%), and a relatively high proportion of minerals (92%) were also observed in some cores, with glass fragments down to 0 vol% (Fig. 3j). A detailed overview of the point counting is provided in supplementary table B.

Glass shard major element compositions

Glass shard major element compositions of Mt. Etna tephra deposits fall within the Na-alkaline series (i.e., Na_2O-2 > K_2O; Le Bas et al. 1986) and vary from basaltic to mugearitic in Unit E, and from benmoreitic to Na-trachytic in Unit D (Fig. 4A). In comparison with other volcanic provinces of the Mediterranean Sea, Mt. Etna has quite distinct major element compositions with only a few overlaps with Stromboli, Vesuvius, and Vulcano Island (Fig. 4A). For further considerations about the petrogenesis of Italian volcanic rocks, the interested reader is referred to Schiano et al. (2004) and references therein.

Glass shards of Unit D deposits are significantly more evolved than those of Unit E, as reflected by e.g. SiO_2 contents (Fig. 4A). Unit D products are Na-trachytes (Fig. 4A), while the composition of Unit E is predominantly mugearitic and, to a lesser extent, hawaiitic and basaltic (Fig. 4A). SiO_2 contents are up to ten weight percent (wt%) higher for Unit D, at ~ 62 wt%, while the SiO_2 content of Unit E are about 52 wt% (Fig. 5). One exception is FS, whose SiO_2 content is about 49 wt% (Fig. 5). For FeO_t, TiO_2, CaO, and MgO, Unit D deposits have lower concentrations (up to 6 wt% for FeO_t, 1.5 wt% for TiO_2 and 0.6 wt% for P_2O_5) than Unit E. The newly obtained chemical data is used to construct correlation fields for further comparison with the marine tephra inventory, which is shown in Fig. 5.

Although the layers of Unit E exhibit considerable geochemical similarity, they can be readily distinguished from one another. For instance, the FS layer is markedly distinct from the remaining layers, exhibiting significantly lower SiO_2 (48.5 to 49.5 wt%) and TiO_2 (1.2 to 1.4 wt%) and higher CaO (approximately 13 wt%) and MgO (6 to 7 wt%). The FL layer has SiO_2 values of up to 57 wt%, while the TV layer is one of the layers with the lowest SiO_2 values (up to

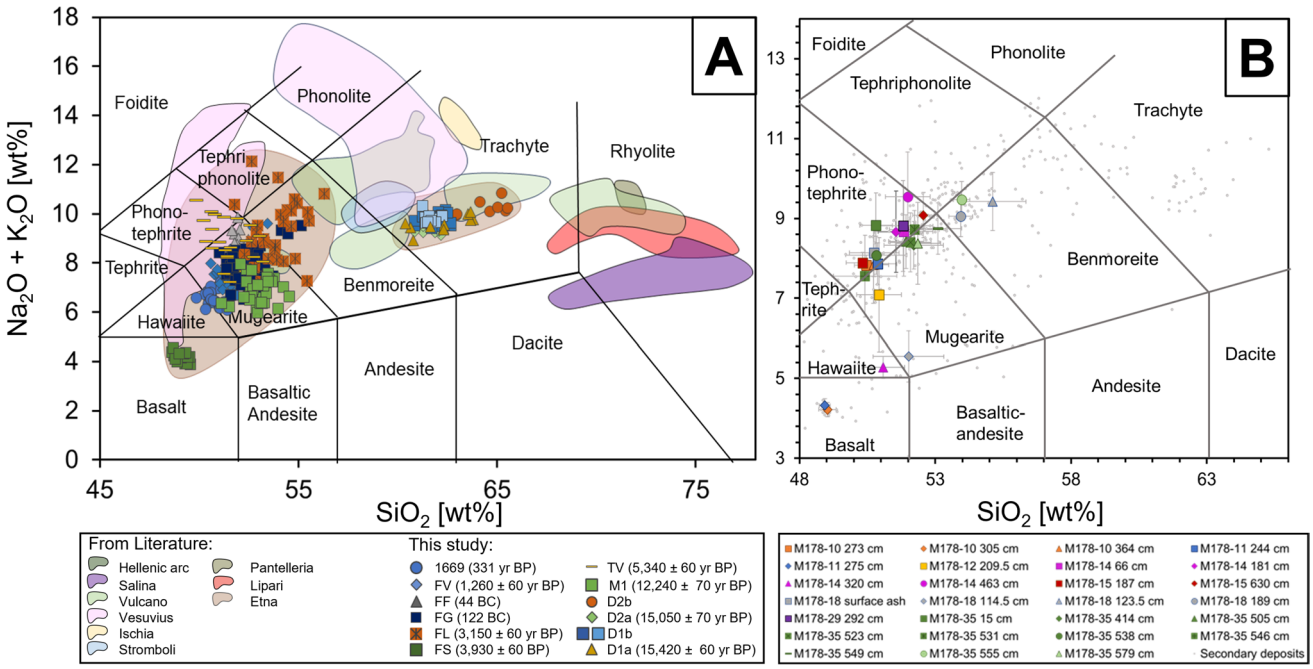

Fig. 4 Total alkalis versus silica classification diagram after Le Maitre et al. (1989). **A** Glass compositional variability of Italian Holocene sources (colored fields) modified after Menke et al. (2018), Albert et al. (2017), and Tomlinson et al. (2015). Symbols represent new data of single measurements obtained in this study. **B** Average glass shard compositions with standard deviations of the primary marine tephra layers of cores M178-10, −11, −12, −14, −15 −18, −29, and −35 (colored symbols). Single glass shard analyses of all secondary marine tephra layers (gray dots)

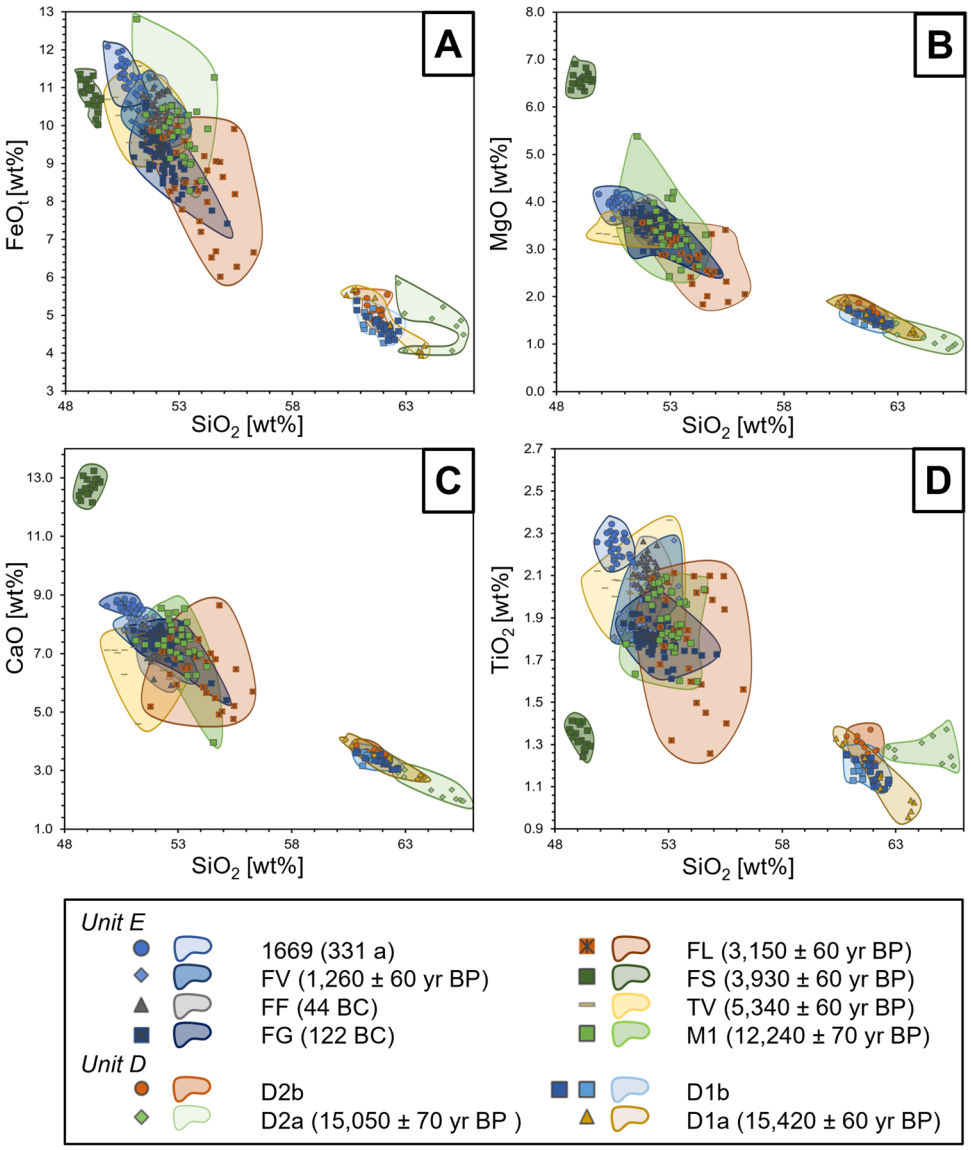

Fig. 5 Major element glass shard analyses of terrestrial marker beds. **A** FeO_t, **B** MgO, **C** CaO, and **D** TiO_2 in wt% versus SiO_2. Symbols represent single glass shard analyses of the individual deposits that were used to build the respective correlation fields (colored fields)

50 wt%). In view of their geochemical overlap, the stratigraphic order of the deposits of course plays an important role in differentiating them from each other.

The investigated marine tephra layers show a widespread variability in glass shard compositions; with the majority having phonotephritic, mugearitic, benmoreitic, and minor hawaiitic and basaltic glass shard compositions, and some samples with tephriphonolitic, phonolitic, and Na-trachytic glass shard compositions (Fig. 4B).

Discussion

Primary tephra deposits vs. secondary deposits

The marine tephra layers in the investigated cores collected offshore Mt. Etna were either deposited as primary or secondary deposits. Primary deposits are defined as syn-eruptive and thus directly related to an explosive volcanic eruption, while secondary deposits are not directly related to an eruption, but rather to post-eruptive re-deposition processes. A primary deposit can either be deposited by a fall or flow process (e.g., pyroclastic density currents), whereas secondary deposits are generally formed by flow processes (e.g., turbidites). For the identification of time markers in the marine sediment record, it is extremely important to distinguish between primary and secondary deposits, since only primary, syn-eruptive deposits provide discrete time markers. The depositional environment offshore Mt. Etna volcano is complex and turbidity currents are common. The presence of turbidites, which might contain reworked material, but can also be related to primary events, makes stratigraphic approaches in the Ionian Sea challenging (Köng et al. 2016). Köng et al. (2016) suggest three trigger mechanisms that

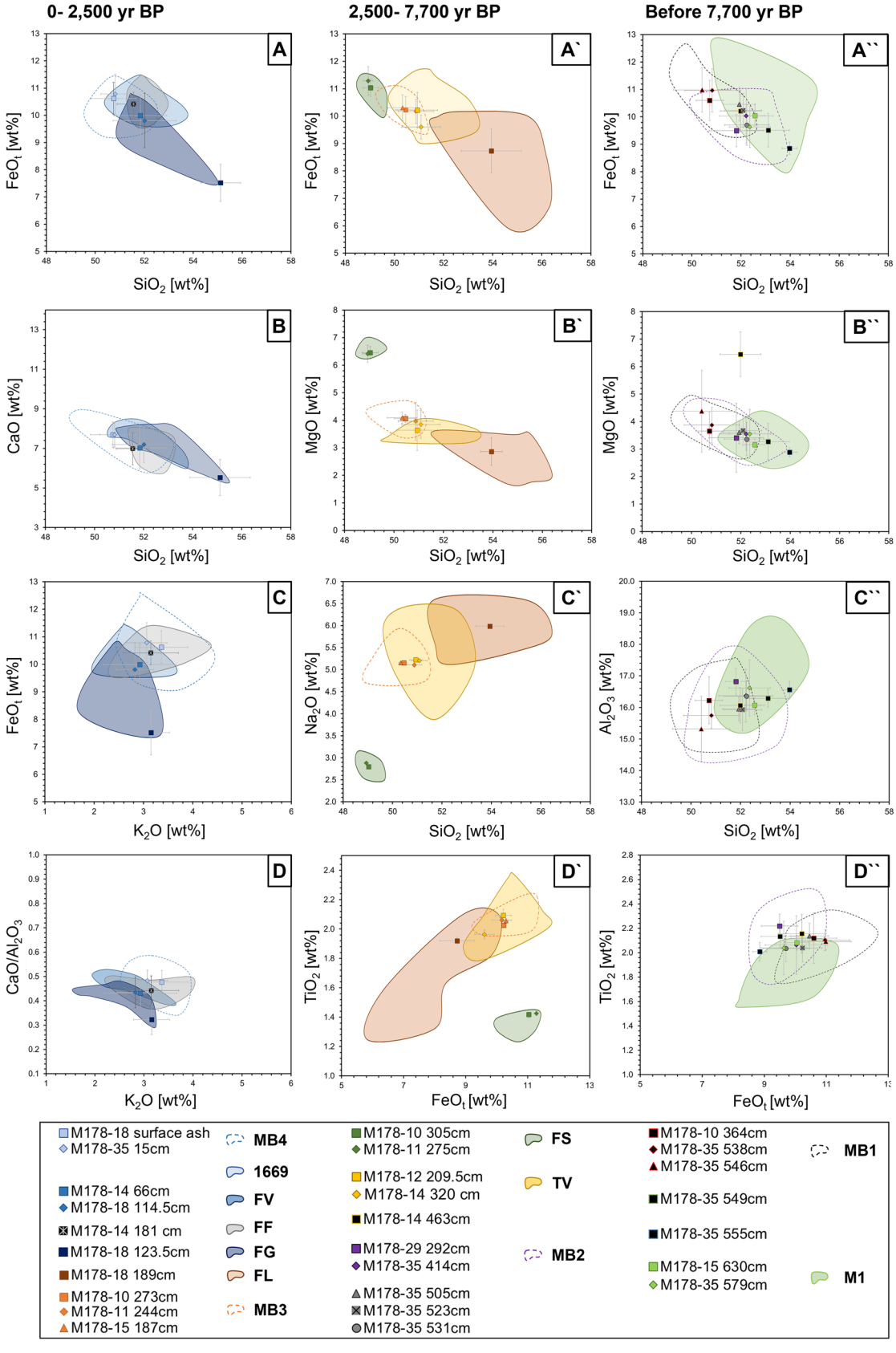
0- 2,500 yr BP
2,500- 7,700 yr BP
Before 7,700 yr BP
A
A`
A``
B
B`
B``
C
C`
C``
D
D`
D``
FeOt [wt%]
SiO2 [wt%]
CaO [wt%]
MgO [wt%]
K2O [wt%]
Na2O [wt%]
Al2O3 [wt%]
CaO/Al2O3
TiO2 [wt%]
M178-18 surface ash
M178-35 15cm
M178-14 66cm
M178-18 114.5cm
M178-14 181 cm
M178-18 123.5cm
M178-18 189cm
M178-10 273cm
M178-11 244cm
M178-15 187cm
MB4
1669
FV
FF
FG
FL
MB3
M178-10 305cm
M178-11 275cm
M178-12 209.5cm
M178-14 320 cm
M178-14 463cm
M178-29 292cm
M178-35 414cm
M178-35 505cm
M178-35 523cm
M178-35 531cm
FS
TV
MB2
M178-10 364cm
M178-35 538cm
M178-35 546cm
M178-35 549cm
M178-35 555cm
M178-15 630cm
M178-35 579cm
MB1
M1

◂**Fig. 6** Correlation fields of the terrestrial marker beds (colored fields) together with average compositions of marine primary tephra layers. **A** + **A`** + **A``** $FeO_t$ vs. $SiO_2$, **B** CaO vs. $SiO_2$, **B`** + **B``** MgO vs. SiO_2, **C** FeO_t vs. K_2O, **C`** Na_2O vs. SiO_2, **C``** $Al_2O_3$ vs. $SiO_2$, **D** $CaO/Al_2O_3$ vs. $K_2O$, **D`** + **D``** TiO_2 vs. FeO_t in wt%. **A**–**D** Tephra layers younger than 72,500 yr BP. **A`**–**D`** Tephra layers between 2500 and 7700 yr BP and **A``**–**D``** Tephra layers older 7700 yr BP. Symbols are averages per sample with standard deviations

could be responsible for turbidite formation in the study area: (1) siliciclastic turbidites triggered by earthquakes and tsunami waves, (2) volcaniclastic turbidites triggered by eruptions at Mt. Etna, or (3) flank collapses. Co-seismic turbidites might have different recurrence times depending on the location of the core.

Primary deposits are typically massive with a sharp planar base, but may occasionally be planar stratified, and are commonly well-sorted (Freundt et al. 2022). Juvenile particles (glass and magmatic minerals) dominate such primary deposits. Primary fall and flow deposits are typically characterized by homogeneous glass compositions if the erupted source magma had a homogeneous composition. If the erupted magma was compositionally zoned or mixed, the glass compositions reflect a coherent differentiation or mixing trend for all elements (Kutterolf et al. 2008; Gudmundsdóttir et al. 2011; Schindlbeck et al. 2013, 2016, 2018a, b; Eisele et al. 2015; Hopkins et al. 2020).

A typical secondary deposit has an erosive basal contact and wavy or cross-bedding of the (poorly sorted) volcaniclastic deposit (Freundt et al. 2022). Secondary turbidites are characterized by having a large fraction of non-volcanic clasts, subaerially weathered or altered (volcanic) clasts (Fig. 3j), and shallow-water bioclasts (Freundt et al. 2022). Secondary volcaniclastic deposits, which are derived from the collapse or erosion of larger sections of volcanic stratigraphy, however, comprise glass compositions that are not immediately genetically related and can thus show a relatively wide, heterogeneous scatter, and clasts may be subrounded to rounded (Kutterolf et al. 2008; Gudmundsdóttir et al. 2011; Schindlbeck et al. 2013, 2016, 2018a, b; Eisele et al. 2015; Hopkins et al. 2020).

Based on these criteria, we classify 27 marine tephra layers as primary deposits, whereas the other 60 layers are interpreted as the result of secondary depositional processes. Figure 6 presents the geochemical compositions of the deposits classified as primary, arranged according to the cores in which they were discovered. The next section describes the age constraints that are included for clarity in Fig. 6. Table 2 summarizes the results for each core and demonstrates clearly that cores taken from morphological depressions (M178-12, M178-14; Fig. 1) have a relatively high proportion of secondary deposits compared to the total number of samples taken. However, it is additionally evident that cores M178-29 and M178-35, despite not being taken from depressions, also have a relatively high proportion of secondary deposits. This may be attributed to the dominance of the sapropel in these cores. A contrasting depositional environment may have prevailed during the time of sapropel formation and thus also have a causal connection to redeposition of tephra layers. This was not the case for the majority of the other cores. For all further geochemical investigations, we concentrate on the 27 primary tephra layers.

Age model

Sedimentation rates were determined following the method described by Kutterolf et al. (2021). The hemipelagic sedimentation rates were constrained from well-correlated and dated tephra layers and the age of the sapropel S1 (10 to 7.7 ka BP) after Checa et al. (2020) bracketing hemipelagic sediment intervals (Figs. 7 and 8; supplementary table G). There are three sediment cores (M178-15, −29, −35) in which the whole sapropel interval was recovered (Figs. 7 and 8); all other cores end within the sapropel. Where available, we preferred tephra time markers in our calculations because it is unclear if sapropels comparatively close to the shore within the Ionian Sea are perfectly synchronous with those of the model calculations of Checa et al. (2020). Primary tephra layers correlated to dated onshore deposits provide the best time markers in the cores, and the ages have the uncertainty of radiometric dating. We used these time markers, without including the errors from radiometric dating, to calculate the average apparent sedimentation rates of the intercalated hemipelagic sediment (Kutterolf et al. 2021). We did not subtract the thickness of intercalated ash beds, as these beds are typically thin (< 10 mm) and cumulatively account for less than 5% of the core length. By applying linear interpolation, we assume that the hemipelagic sedimentation rate between time markers remained constant over time, which enables us to calculate ages for undated tephra layers between those tie points. Uncertainties in the sedimentation rate arise from this linear interpolation, as well as initial radiometric dating errors for the dated tephras (Kutterolf et al. 2021). The ^{14}C age from M178-14, 330 cm (5775 ± 35 yr BP), which corresponds to a calibrated age of 6487–6666 yr cal BP, agrees well with the ages obtained from tephra time markers.

Figure 8 shows the age model and sedimentation rates of the cores that represent the entire sapropel. Core M178-35 has an average sedimentation rate of 44 cm/kyr above the sapropel, while the sapropel has a sedimentation rate of 103 cm/kyr. M178-29 has a sedimentation rate of 30 cm/kyr, but within the sapropel, it increases to 100 cm/kyr. In the M178-15 core, the sedimentation rate is 52 cm/kyr above the sapropel. The sedimentation rate within the sapropel sharply rises to 147 cm/kyr.

Table 2 Total number of samples that were taken from the respective cores of M178, together with the number of samples identified as primary and secondary deposits and the geochemical composition of the primary deposits

Core # from M178	Total samples taken	Layers identified as primary deposit	Layers identified as secondary deposit	Composition of primary deposits
10	3	3	0	Phonotephritic
11	4	2	2	Basaltic to phonotephritic
12	7	1	6	Mugearitic
14	18	2	16	Mugearitic, phonotephritic
15	4	2	2	Basaltic, phonotephritic
18	7	4	3	Phonotephritic, mugearitic, benmoreitic
29	21	1	20	Phonotephritic
35	26	10	16	Phonotephritic, mugearitic, benmoreitic

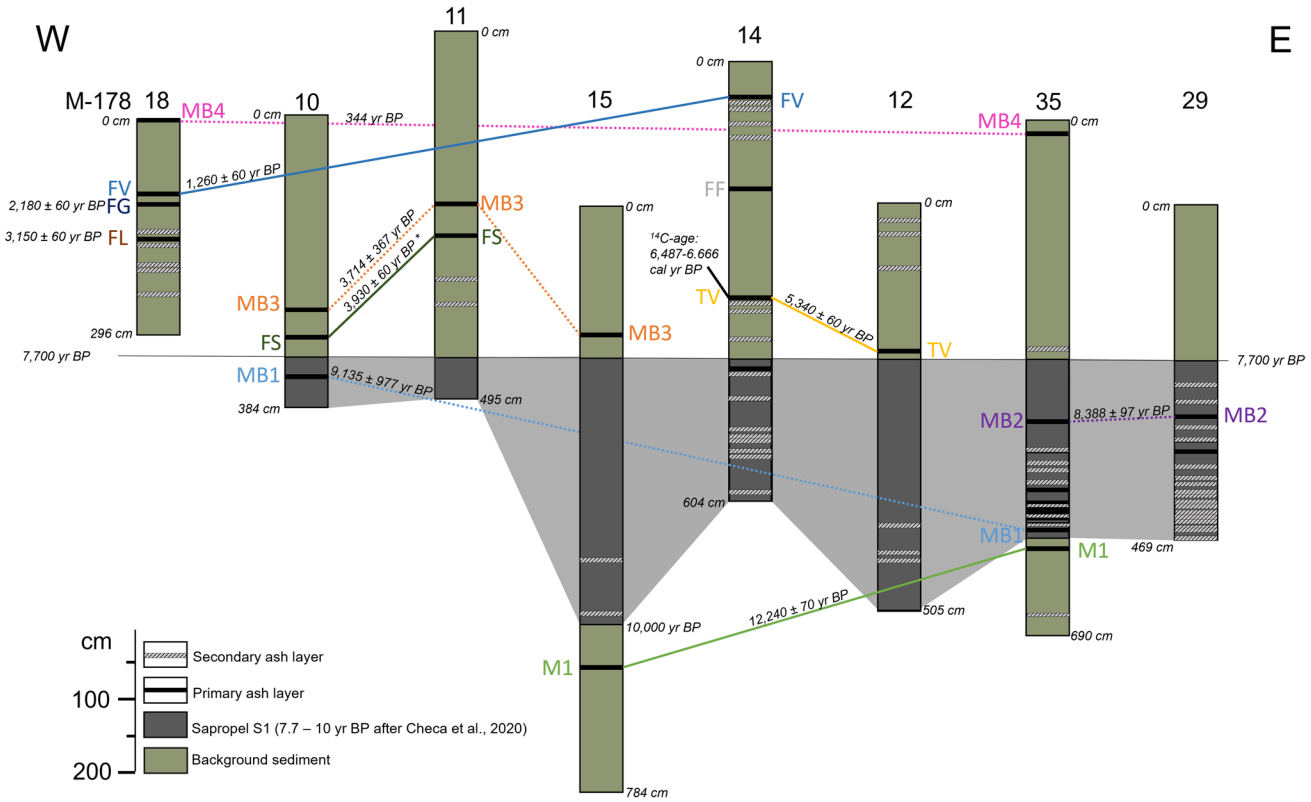

Fig. 7 West-to-East composite profile of the marine cores (M178-18, −10, −11, −15, −14, −12, −35, and −29). The primary deposits with onshore/offshore and offshore/offshore correlations and secondary deposits are shown, as well as the position of sapropel S1 (in gray)

However, it should be noted that although the cores are located within a small area of about 99 km^2, the depths of the sapropel within the sediment cores are quite variable. This is partly because the cores are of different lengths, but also because some cores were taken on ridges (e.g., on top of the amphitheater), which is the case for cores M178-15, −29 and −35 (Fig. 1A), while other cores were taken in morphologic depressions (e.g., inside the amphitheater, M178-12 and −14). Another important factor is the distance to the coast. While core M178-15 is only 9 km from the coast and lies directly on a ridge above the amphitheater, the other two cores are much further away from the coast. M178-29 is 30 km from the coast and lies much further south of the amphitheater. M178-35, on the other hand, is about 15 km from the coast and lies further north. It can be reasonably assumed that sedimentation rates fluctuate more closer to the coast due to significantly more variable sediment input (see core M178-15). Cores located further away from the coast exhibit more uniform

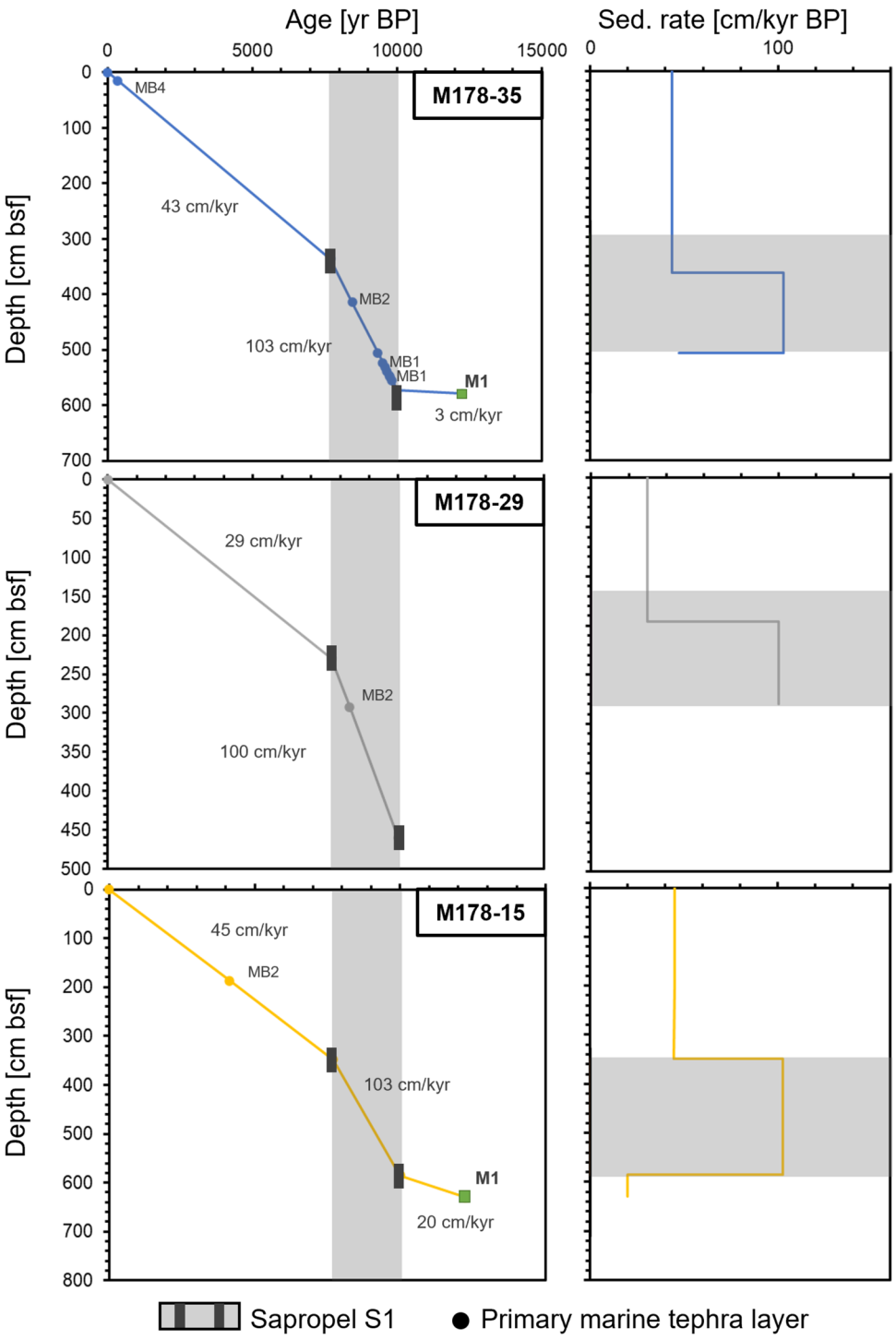

Fig. 8 Sediment thickness versus age for selected M178 cores. Right part of each age profile shows the variation of sedimentation rate with depth in cm below the sea floor (cm bsf), tephra thicknesses excluded. Sapropel S1 is marked in gray

rates. Nevertheless, the time period of the sapropel clearly shows a strong increase in sedimentation rates in all cores.

The input of sediment and mass flow deposits for those cores taken in depressions is significantly higher than for those on ridges. This makes the age determination of the sapropel and deposits more complicated for the cores M178-12 and −14.

Correlation of primary tephra layers

The 27 primary marine tephra layers were investigated in detail and correlated to known terrestrial eruptions. We use bivariate plots of major elements and their ratios to identify the terrestrial counterparts of the marine deposits (Fig. 6). In addition to the geochemical compositions, we also use

stratigraphical constraints, as well as macroscopic and microscopic observations, to validate the established correlations. In total, we correlate eleven of the marine tephra layers from seven cores to seven well-known terrestrial layers. Additionally, we are able to correlate another four layers between two or more marine cores (ten core samples). The four layers correlated core-to-core are named MB1 to MB4, after Mongibello (MB), the alternative name of Mt. Etna. Six primary marine tephra layers are not correlated to known onshore deposits and also not between cores, which means that, in sum, we have 17 primary volcanic events identified within the marine sediments.

Onshore-offshore correlations

M1 layer Marine tephra layers M178-15, 630 cm and M178-35, 579 cm can be geochemically correlated to the 12,240 ± 60 yr BP M1 eruption (Coltelli et al. 2000) (Figs. 6A´´, B´´, C´´, D´´). The tephra is characterized by high FeO_t contents of up to 13 wt%. The marine tephra layers have a sharp, partly erosive basal contact, which indicates that they might be deposited as a flow in the marine environment. Point counting revealed a relatively high proportion of juvenile components (17%) in comparison to the proportion of organic material and other volcanic particles (supplementary table B). Both layers are deposited below the sapropel S1 (Fig. 7), which agrees well with the age of the M1 eruption.

TV layer M178-12, 209.5 cm and M178-14, 320 cm can be assigned to the TV eruption based on geochemical characteristics such as high TiO_2 (up to 2.4 wt%) (Fig. 6A´, B´, C´, D´)). The TV eruption is dated to 5430 ± 60 yr BP (Coltelli et al. 2000), which is slightly younger than the sapropel S1. This agrees very well with the position just above the sapropel in the core (Fig. 7, supplementary table B).

FS layer Marine tephra layers M178-10, 305 cm and M178-11, 275 cm (Figs. 6 and 7, supplementary table B) are correlated to the FS eruption, which is dated to 3930 ± 60 yr BP (Coltelli et al. 2000, 2005; Malaguti et al. 2023). The FS layer is easily distinguishable due to the high MgO content of up to 7 wt%, low Na_2O content (2.5 to 3.3 wt%), and SiO_2 of 49 to 50 wt% (Fig. 6).

FL layer The geochemical composition of the FL layer (3150 ± 60 yr BP; Coltelli et al. 2000) exhibits significant variability, with FeO_t values ranging from 5.5 to 9.5 wt% and SiO_2 values from 51 to 56 wt%. Nevertheless, it is quite similar to the FG layer and shows strong overlap, particularly with regard to silica. Two primary layers, M178-18, 123.5 cm (Fig. 6) and 189 cm (Fig. 6), exhibit notable similarities in their geochemical composition to both FL and FG. However, we have correlated layer M178-18, 189 cm to the FL layer, as this layer is stratigraphically deposited at a greater depth within the core and exhibits a closer match in terms of geochemical characteristics (Fig. 7, supplementary table B).

FG layer The FG marker bed (2180 ± 60 yr BP; Coltelli et al. 2000) is characterized by slightly higher SiO_2 (51 to 56 wt%) content and a comparatively low FeO_t content of 7.4 to 10.8 wt% with respect to the other layers of Unit E (Fig. 6). We propose that the upper layer M178-18, 123.5 cm is the FG layer, based on the stratigraphic position and age calculations (supplementary table B). Nonetheless, the doublet of primary layers recovered in core M178-18 suggests that there were actually two eruptive events within 1000 years with very similar compositions, possibly representing both the FL and the FG layers (Fig. 7).

FF layer The FF layer (2044 ± 60 yr BP; Coltelli et al. 2000) is geochemically very similar to other deposits of the Unit E and overlaps with their reference fields (Fig. 6), so stratigraphy was used to correlate the marine tephra layers. The deposit M178-14, 181 cm (Figs. 6 and 7) was correlated to the FF layer based on its relative position within the sediment core, as well as its geochemical composition of slightly elevated K_2O content of average 3.2 wt% and slightly lower CaO content of average 7 wt% (supplementary table B).

FV layer The FV layer (1260 ± 60 yr BP; Coltelli et al. 2000) is very similar to the FF layer and its reference field overlaps with the reference fields of other deposits of Unit E. Marine tephra layers M178-14, 66 cm (Fig. 7) and M178-18, 114.5 cm (Fig. 6) were correlated to the FV layer based on the relative stratigraphic position of the deposits within the sediment cores (Fig. 7, supplementary table B).

Offshore-offshore correlations

We also used glass shard geochemical compositions to correlate tephra beds between the marine cores. The layers that we were able to correlate with each other, and which thus describe the same event, are here called MB1 to MB4 (Fig. 7). The glass compositions from these ash layers are all similar to those of Unit E, which suggests that these were erupted within the Mongibello Phase of Mt. Etna.

Correlation of deposits younger than 7700 a Based on their geochemical compositions, two primary tephra layers (M178-18, 0 cm (top of the core) and M178-35, 15 cm) can be correlated in the uppermost sections of the cores. Due to their position in the cores their age is younger than 1260 yr BP. They have a phonotephritic composition with FeO_t contents of 11 wt% and SiO_2 contents of about 51 wt%,

respectively, and we refer to these tephra layers as MB4 (Fig. 6).

Three phonotephritic marine layers (M178-10, 273 cm, M178-11, 244 cm, and M178-15, 187 cm) are younger than 3930 yr BP and can be correlated between the cores (called MB3; Fig. 6) based on their geochemical composition and stratigraphic position above the geochemically distinctive FS layer in two of the three core (Fig. 7). Applying sedimentation rates, the calculated age is about 3500 ± 80 yr BP. We cannot correlate these deposits with any terrestrial beds. According to Coltelli et al. (2000), there are two fine lapilli beds deposited above FS, named S8 and S9, which may correlate with our marine deposits. However, there is no reference sample material or geochemical data available for reliable correlations.

Correlation of deposits older than 7700 a In general, it is necessary to state that both the distinction into primary and secondary deposits, and correlation of deposits identified as primary within the sapropel (between 10 and 7.7 ka BP) is particularly difficult due to the compositional similarity and the periodically varying depositional environment. A total of 11 primary tephra layers were deposited within sapropel S1, giving an age range between 10 and 7.7 ka BP (Fig. 7). In total, two correlations involving five marine tephra layers can be established within this age range, named MB1 and MB2 (Figs. 6 and 7).

For event MB1, we correlated M178-10, 364 cm and M178-35, 546 cm. MB1 has a phonotephritic to mugearitic composition. An age of 9135 ± 979 yr BP was calculated for MB1 based on sedimentation rates (Fig. 8, Table 3). A second tephra layer in core M178-35 (M178-35, 538 cm) is compositionally very similar to those two deposits, with FeO_t of 11 wt% and SiO_2 of 51 wt%, respectively. However, this tephra layer has an erosional base contact and is therefore likely a flow deposit. Based on the sedimentary features, we propose that the M178-35, 546 cm is the correlative deposit, but we cannot rule out that the upper layer M178-35, 538 cm is the actual deposit of MB1.

The MB2 event is based on a correlation between marine tephra layers M178-29, 292 cm and M178-35, 414 cm, because both have similar glass compositions (phonotephritic to mugearitic) and similar stratigraphic positions (Figs. 4B and 7). Below M178-35, 414 cm, we found three additional layers similar to this sample. However, as these are stratigraphically far below the deposit in the other core, it is possible that these flow deposits belong to an additional eruption that is geochemically very similar to MB4. MB2 has a calculated age of 8388 ± 97 yr BP and a tephriphonolitic composition (Table 3).

Additionally, there are six single site primary layers that cannot be correlated to known terrestrial deposits or to another primary marine tephra layer. Marine tephra layer M178-14, 463 cm, with a calculated age of about 7726 yr BP, has a phonotephritic composition (Fig. 4B), and a sharp basal contact to the background sediment (supplementary table B). The other five are thin (< 1 cm thickness) single site tephra layers in core M178-35 at depths 505 cm, 523 cm, 549 cm, and 555 cm with calculated ages between 9340 and 9825 yr BP, all showing erosive basal contacts (supplementary table B).

Table 3 Primary marine tephra layers with their correlated eruptions and the respective ages. Ages marked with the star are from Coltelli et al. (2000). No star indicates that the ages that are calculated with the age model from this study

Marine sample	Correlated eruption	Ages [yr BP]
M178-18 surface ash	MB4	344
M178-35 15 cm	MB4	344
M178-14 66 cm	FV	1260 ± 60*
M178-18 114.5 cm	FV	1260 ± 60*
M178-14 181 cm	FF	2044 ± 60*
M178-18 123.5 cm	FG	2180 ± 60*
M178-18 189 cm	FL	3150 ± 60*
M178-10 273 cm	MB3	3714 ± 367
M178-11 244 cm	MB3	3714 ± 367
M178-15 187 cm	MB3	3714 ± 367
M178-10 305 cm	FS	3930 ± 60*
M178-11 275 cm	FS	3930 ± 60*
M178-12 209.5 cm	TV	5340 ± 60*
M178-14 320 cm	TV	5340 ± 60*
M178-14 463 cm		7726
M178-29 292 cm	MB2	8388 ± 97
M178-35–414 cm	MB2	8388 ± 97
M178-35–505 cm		
M178-35–523 cm		
M178-35–531 cm		
M178-10 364 cm	MB1	9135 ± 977
M178-35–538 cm	MB1	9135 ± 978
M178-35–546 cm	MB1	9135 ± 979
M178-35–549 cm		9767
M178-35–555 cm		9825
M178-15 630 cm	M1	12,240 ± 70*
M178-35 579 cm	M1	12,240 ± 70*

Correlations to distal sources and sediment archives

FL as a widespread marker horizon The FL tephra (3150 ± 60 yr BP) from Mt. Etna is a widely dispersed deposit that was previously discovered as tephra layers and cryptotephra in distal sediment archives in Lake Ohrid and Lake Shkodra (Albania-Macedonia) as well as in the more proximal sediment cores recovered in Lago di Perguso in central Sicily (Wagner et al. 2008; Vogel et al. 2010;

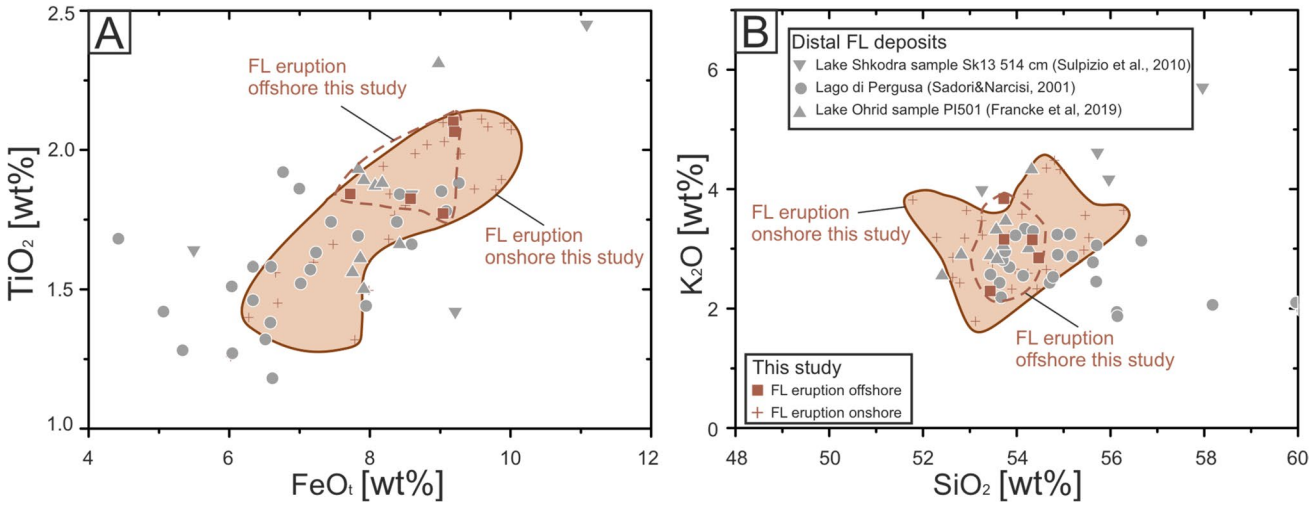

Fig. 9 Single glass shard compositions. **A** FeO_t versus TiO_2 plot and **B** SiO_2 versus K_2O plot for comparison of marine (brown squares) and onshore FL data (brown correlation field) of the 3150 ± 60 yr BP FL tephra from this study with data from distal deposits in Lake Ohrid, Lake Shkodra, and more proximal Lago di Pergusa (Francke et al. 2019; Sulpizio et al. 2010; Sadori & Narcisi 2001)

Sulpizio et al. 2010; Sadori and Narcisi 2001) (Fig. 9). It is therefore used as an important time marker in the Mediterranean (e.g., Francke et al. 2019). Interestingly, in the investigated cores, we only detected the marine deposits of the FL event in the most proximal core M178-18 (Figs. 1 and 7) and although the correlation field of the FL deposit is rather large and overlaps with some of the other Mt. Etna correlation fields (Figs. 5 and 6), especially the FeO_t versus SiO_2 diagram, is useful to distinguish between FL and the other Mt. Etna deposits, since the FL deposit tends to higher SiO_2 at lower FeO_t contents (Fig. 5A). The MB3 layer is in a suspicious stratigraphic position as it occurs in two cores just above the geochemically distinct FS layer (Fig. 7); however, the geochemical composition of MB3 is different from what is known from FL, with lower SiO_2 (< 51 wt%) and relatively high FeO_t (> 10 wt%) and CaO contents (> 8 wt%) (Fig. 6). Sulpizio et al. (2010) proposed a rather narrow eruption cloud with a north eastward direction, which might explain why our marine cores east of Mt. Etna lack the FL deposits.

Medieval-first eruption in M178 cores? The tephra layers of the MB4 event are the youngest deposits within the investigated marine tephra record offshore Mt. Etna (Fig. 7, Table 3). They are younger than 1260 yr BP and probably older than the 1669 Mt. Etna eruption. It is probable that they correspond to one of the N11 to N16 eruptions of Mt. Etna (Fig. 2; Del Carlo et al. 2004). However, there is no sample material or geochemical data available that allow us to evaluate this possibility further. Another potential source volcano for an eruption at this time is Somma-Vesuvius with the 1265 yr BP "Medieval first" eruption (Simkin and Siebert 2005). The age of the tephra samples agrees well with the age of this eruption, at 1260 yr BP. However, due to the lack of correlative data, this remains speculative.

Implications for Mt. Etna volcanic activity

We correlated eleven marine tephra layers to seven marker beds on land and discovered ten additional eruptions, indicating that Mt. Etna has been more active than previously thought during the time of the deposition of the sapropel S1 between 10 and 7.7 ka BP. Del Carlo et al. (2004) state that the explosive activity of Mt. Etna was very low or absent for a period of about 3 kyr after the Ellittico caldera-forming eruptions. Unit E started with deposition of the M1 bed, produced by a large Subplinian eruption at about 12 ka, which we found within our marine cores (M178-15, 630 cm and M178-35, 579 cm). At least 10 deposits produced by Subplinian eruptions between 12 and 7.5 ka have been found onshore (Del Carlo et al. 2004). The formation of the sapropel S1 is also documented within this time period (10 to 7.7 ka BP) by Checa et al. (2020) for the Ionian Sea. As the marine study area of this work is located further south and in a quite different sedimentary and tectonic environment compared to that of Checa et al. (2020), the time limits of the sapropel may be different from those suggested by those authors. The uncertainty in age and correlation of primary tephra layers within the sapropel thus remains a problem in the construction of robust tephrostratigraphy for Mt. Etna. In any case, the presence of 11 primary tephra layers within the sapropel, erupted from Mt. Etna between 10 and 7.7 ka BP, proves that there was considerable explosive activity

within this time interval. Del Carlo et al. (2004) further show that in the following 2000 years, between about 7.5 ka BP and deposition of the TV layer (5340 ± 60 yr BP), the volcaniclastic succession is represented by 1–2-m-thick eolian deposits in which the record of the explosive activity is scarce. Since we have neither exact age dating for the sapropel nor for marine tephra layers within the sapropel near the east coast of Sicily, it is also conceivable that the age of the sapropel S1 and of the tephra layers are significantly younger than what we have roughly calculated (Table 3). However, no deposits from eruptions of Mt. Etna have been found on land in this younger age range to date. The Milo lahar unit, which includes a debris-avalanche deposit related to the opening of VdB (Calvari et al. 1998), is covered by the TV layer. This constrains the timing of the VdB formation. What is striking is that the deposits of Unit E (last 12 kyr) mantle the flanks of Mt. Etna continuously from the summit to the distal areas, but are completely absent in the Valle del Bove floor (Coltelli et al. 2000), which lies in the main wind direction from the volcano. This raises the question of whether any deposits in this region were transported deeper into the Ionian Sea when the valley was opened up, or whether deposits were lost or eroded in this process. In any case, this underlines the importance of the marine sediment archives to unravel the (explosive) volcanic history of Mt. Etna.

Del Carlo et al. (2004) further state that during the 1400 years between deposition of the TV and the FS units, the explosive activity weakened, producing few widely dispersed tephra layers. A very intense period of explosive activity began with the FS Subplinian eruption (3930 ± 60 yr BP; Coltelli et al. 2000). Afterwards, the frequency and magnitude of explosive eruptions dramatically increased compared to the previous 8000 years and has remained elevated until the present. Moreover, in the last 4000 years, two of the largest Holocene explosive eruptions of Mt. Etna occurred. The first one formed the FL layer at 3150 ± 60 yr BP (Coltelli et al. 2000) and the second one formed the deposit of the 122 BC Plinian eruption (FG marker bed) (Del Carlo et al. 2004). Apart from the large FS, FL and FG eruptions, many mid-intensity explosive eruptions (mainly Subplinian) have occurred at Mt. Etna over the last 4000 years (about 7 per ka; Del Carlo et al. 2004).

However, it is also possible that Mt. Etna was more active during the time of the sapropel S1 deposition between 10 and 7 ka BP than previously concluded, based on the tephrostratigraphic studies (e.g., Coltelli et al. 2000; Del Carlo et al. 2004; Branca and Del Carlo 2004). In particular, the newly correlated deposits MB1 and MB2, as well as other primary layers found at the beginning of the Holocene between 10 and 7 ka BP, give us deeper insight into the geological evolution of Mt. Etna by providing more information about eruptive processes, the explosivity and magnitudes of eruptions, and especially the processes that occurred offshore before, during, and in the millennia following each event.

Conclusions

In this work, we build a marine tephrostratigraphic framework by studying eight gravity cores taken offshore Mt. Etna and investigating 87 marine tephra layers within the cores. Based on volcanic glass shard geochemistry and petrographic observations, we identified 27 primary pyroclastic deposits. Applying geochemical fingerprinting, we correlated eleven of the primary deposits to seven well known eruptions of Mt. Etna, which provide valuable time markers in the marine sediment records and comprise the FV, FF, FG, FL, FS, TV, and M1 eruptions. Another ten primary tephra layers have been correlated between cores, which enlarge the tephrostratigraphic framework significantly. Together with the remaining six single-site tephra layers, we discovered 17 volcanic events that must have been widespread and large enough to reach the distal coring sites. It is noteworthy that we discovered six eruptions within the time span from 10 to 7 ka BP, i.e., within the sapropel S1 time period. This study demonstrates the value of integrating terrestrial and marine data sets to enhance the understanding of the eruption history of a volcano such as Mt. Etna. However, further studies are necessary to deepen these insights and to provide a more comprehensive picture from a marine perspective.

Supplementary Information The online version contains supplementary material available at https://doi.org/10.1007/s00445-024-01785-x.

Acknowledgements We acknowledge the support from the Istituto Nazionale di Geofisica e Vulcanologia, Osservatorio Etneo (INGV) in Catania, providing vehicles and fieldwork materials. We also thank GEOMAR Helmholtz Centre for Ocean Research in Kiel, especially Mario Thöner, for his assistance with the electron microprobe analytics. Additionally, we appreciate the support of the crew of RV Meteor during cruise M178. We are thankful to Ralph Schneider, Kiel University, for providing the ^{14}C dating.

Funding Open Access funding enabled and organized by Projekt DEAL. The *RV Meteor* expedition M178 was evaluated and funded by the Deutsche Forschungsgemeinschaft (DFG, German Research Foundation) grant number GPF 21-2_061. Morelia Urlaub received funding by the Helmholtz Association's Initiative and Networking Fund (Young Investigator Group) VH-NG-1617.

Data availability All geochemical glass analyses obtained by electron microprobe, including standard analyses, are provided as supplementary material.

Code availability Not applicable.

Declarations

Competing interests The authors declare no competing interests.

References

Albert PG, Tomlinson EL, Lane CS, Sabine Wulf VC, Smith M, Coltelli JK et al (2013) Late glacial explosive activity on Mount Etna: implications for proximal–distal tephra correlations and the synchronisation of Mediterranean archives. J Volcanol Geotherm Res 265:9–26 (**Elsevier**)

Albert PG, Tomlinson EL, Smith VC, Di Traglia F, Pistolesi M, Morris A, Donato P, De Rosa R, Sulpizio R, Keller J et al (2017) Glass geochemistry of pyroclastic deposits from the Aeolian Islands in the last 50 ka: a proximal database for tephrochronology. Elsevier 336:81–107 (**Elsevier**)

Allan ASR, Baker JA, Carter L, Wysoczanksi RJ (2008) Reconstructing the Quaternary evolution of the world's most active silicic volcanic system: insights from an 1.65 Ma deep ocean tephra record sourced from Taupo Volcanic Zone, New Zealand. Quatern Sci Rev 27:2341–2360 (**Elsevier**)

Ariztegui D, Asioli A, Lowe JJ, Trincardi F, Vigliotti L, Tamburini F, Chondrogianni C, Accorsi CA, Mazzanti MB, Mercuri AM et al (2000) Palaeoclimate and the formation of sapropel S1: inferences from Late Quaternary lacustrine and marine sequences in the central Mediterranean region. Palaeogeogr Palaeoclimatol Palaeoecol 158(3–4):215–240

Behncke B, Branca S, Corsaro RA, De Beni E, Miraglia L, Proietti C (2014) The 2011–2012 summit activity of Mount Etna: birth, growth and products of the new SE crater. Edited by Elsevier. J Volcanol Geotherm Res 270:10–21

Bisson M, Del Carlo P (2013) A GIS-based application for volume estimation and spatial distribution analysis of tephra fallout: a case study of the 122 BC Etna eruption. Ann Geophys 56(1):R0105–R0105

Branca S, Coltelli M, Groppelli G, Lentini F (2011) Geological map of Etna volcano, 1: 50,000 scale. Ital J Geosci 130:265–291 (**GeoScienceWorld**)

Branca S, Del Carlo P (2004) Eruptions of Mt Etna during the past 3.200 years: a revised compilation integrating the Historical and stratigraphic records. Mt. Etna: volcano laboratory

Bronk Ramsey C (2021) OxCal v4.4.4. Available at: https://c14.arch.ox.ac.uk/oxcal.html

Calvari S, Tanner LH, Groppelli G (1998) Debris-avalanche deposits of the Milo Lahar sequence and the opening of the Valle del Bove on Etna volcano (Italy). J Volcanol Geotherm Res 87:193–209 (**Elsevier**)

Calvari S, Groppelli G, Pasquaré G (1996) The last 100,000 years of Mt. Etna's history as inferred from a geological survey of the south-western wall of the Valle del Bove. Etna: fifteen years on, pp 16–19

Capotondi L, Vigliotti L, Bergami C, Sangiorgi F (2011) The Dark Side of the Mediterranean Geological Record: the sapropel layers and a case study from the Ionian Sea. Marine Research at CNR. Dipartimento Terra e Ambiente—CNR ed. CNR, Roma, pp 658–669

Carlo D, Paola LV, Coltelli M (2004) Last 100 ka tephrostratigraphic record of Mount Etna. Wash DC Am Geophys Union Geophys Monogr Ser 143:77–89

Checa H, Margaritelli G, Pena LD, Frigola J, Cacho I, Rettori R, Lirer F (2020) High resolution paleo-environmental changes during the Sapropel 1 in the North Ionian Sea, central Mediterranean. The Holocene 30:1504–1515 (**SAGE Publications Sage UK: London, England**)

Chiocci FL, Coltelli M, Bosman A, Cavallaro D (2011) Continental margin large-scale instability controlling the flank sliding of Etna volcano. Earth Planet Sci Lett 305:57–64 (**Elsevier**)

Coltelli M, Del Carlo P, Vezzoli L (1998) Discovery of a Plinian basaltic eruption of Roman age at Etna volcano, Italy. Geology 26:1095–1098 (**Geological Society of America**)

Coltelli M, Del Carlo P, Vezzoli L (2000) Stratigraphic constraints for explosive activity in the past 100 ka at Etna Volcano, Italy. Int J Earth Sci 89:665–677 (**Springer**)

Coltelli M, Del Carlo P, Pompilio M, Vezzoli LUIGINA (2005) Explosive eruption of a picrite: The 3930 BP subplinian eruption of Etna volcano (Italy). Geophys Res Lett 32(23)

Del Carlo P, Branca S, D'Oriano C (2017) New findings of Late Glacial Etna pumice fall deposits in NE Sicily and implications for distal tephra correlations in the Mediterranean area. Bull Volcanol 79:1–17

Del Carlo P, Smedile A, Petrelli M, Di Roberto A (2020) Evidence for an unknown explosive eruption of Mt. Etna volcano (Italy) during the Late Glacial. J Volcanol Geotherm Res 402:106992

Derkachev AN, Gorbarenko SA, Ponomareva VV, Portnyagin MV, Malakhova GI, Liu Y (2020) Middle to late Pleistocene record of explosive volcanic eruptions in marine sediments offshore Kamchatka (Meiji Rise, NW Pacific). J Quat Sci 35:362–379 (**Wiley Online Library**)

Doglioni C, Innocenti F, Mariotti G (2001) Why Mt Etna? Terra Nova 13(1):25–31

Eisele S, Reißig S, Freundt A, Kutterolf S, Nürnberg D, Wang KL, Kwasnitschka T (2015) Pleistocene to Holocene offshore tephrostratigraphy of highly explosive eruptions from the southwestern Cape Verde Archipelago. Mar Geol 369:233–250 (**Elsevier**)

Emeis KC, Robertson AHF, Richter C (1996) Shipboard Scientific Party. In: Proceedings of the Ocean Drilling Program, Initial Reports, vol 160

Francke A, Dosseto A, Panagiotopoulos K, Leicher N, Lacey JH, Kyrikou S, ... Leng MJ (2019) Sediment residence time reveals Holocene shift from climatic to vegetation control on catchment erosion in the Balkans. Glob Planet Chang 177:186–200

Freundt A, Schindlbeck-Belo JC, Kutterolf S, Hopkins JL (2022) Tephra layers in the marine environment: a review of properties and emplacement processes. Geol Soc Lond Spec Publ 520:SP520-2021

Grimm R, Maier-Reimer E, Mikolajewicz U, Schmiedl G, Müller-Navarra K, Adloff F, Grant KM, Ziegler M, Lourens LJ, Emeis K-C (2015) Late glacial initiation of Holocene eastern Mediterranean sapropel formation. Nat Commun 6:1–12 (**Nature Publishing Group**)

Gross F, Krastel S, Geersen J, Behrmann JH, Ridente D, Chiocci FL, Bialas J et al (2016) The limits of seaward spreading and slope instability at the continental margin offshore Mt Etna, imaged by high-resolution 2D seismic data. Tectonophysics 667:63–76 (**Elsevier**)

Gross F, Urlaub M, Petersen F, Barett R, Kolling H, Heinrich M, Bonforte A et al. (2021) Cruise Report M178 - HazELNUT. Kiel

Gudmundsdóttir ER, Eiríksson J, Larsen G, (2011) Identification and definition of primary and reworked tephra in Late Glacial and Holocene marine shelf sediments off North Iceland. J Quat Sci 26:589–602 (**Wiley Online Library**)

Guest JE, Murray JB (1979) An analysis of hazard from Mount Etna volcano. J Geol Soc 136:347–354 (**The Geological Society of London**)

Hopkins JL, Wysoczanski RJ, Orpin AR, Howarth JD, Strachan LJ, Lunenburg R, McKeown M, Ganguly A, Twort E, Camp S (2020) Deposition and preservation of tephra in marine sediments at the active Hikurangi subduction margin. Quatern Sci Rev 247:106500 (**Elsevier**)

Hunt JB, Hill PG (2001) Tephrological implications of beam size—sample-size effects in electron microprobe analysis of glass shards. J Quatern Sci: Published Quaterny Res Assoc 16:105–117 (**Wiley Online Library**)

Köng E, Zaragosi S, Schneider J-L, Garlan T, Bachèlery P, Pedro LS, Seibert C, Racine C (2016) Untangling the complex origin of turbidite activity on the Calabrian Arc (Ionian Sea) over the last 60 ka. Mar Geol 373:11–25 (**Elsevier**)

Kutterolf S, Freundt A, Burkert C (2011) Eruptive history and magmatic evolution of the 1.9 kyr Plinian dacitic Chiltepe Tephra from Apoyeque volcano in west-central Nicaragua. Bull Volcanol 73:811–831

Kutterolf S, Schindlbeck JC, Anselmetti FS, Ariztegui D, Brenner M, Curtis J, Schmid D et al (2016) A 400-ka tephrochronological framework for Central America from Lake Petén Itzá (Guatemala) sediments. Quatern Sci Rev 150:200–220 (**Elsevier**)

Kutterolf S, Freundt A, Druitt TH, McPhie J, Nomikou P, Pank K, Schindlbeck-Belo JC, Hansteen TH, Allen SR (2021) The medial offshore record of explosive volcanism along the central to eastern Aegean Volcanic Arc: 2. Tephra ages and volumes, eruption magnitudes and marine sedimentation rate variations. Geochem Geophys Geosyst 22:e2021GC010011 (**Wiley Online Library**)

Kutterolf S, Freundt A, Perez W, Mörz T, Schacht U, Wehrmann H, Schmincke HU (2008) Pacific offshore record of plinian arc volcanism in Central America: 1. Along-arc correlations. Geochem Geophys Geosyst 9(2)

Le Bas MJ, Le Maitre RW, Streckeisen A, Zanettin B (1986) A chemical classification of volcanic rocks based on the total alkali-silica diagram. J Petrol 27(Part 3):745–750

Le Maitre RW, Bateman P, Dudek A, Keller J, Lameyre J, Le Bas MJ, Sabine PA et al (1989) A classification of igneous rocks and glossary of terms. Recommendations of the IUGS subcommission on the systematics of igneous rocks. A classification of igneous rocks and glossary of terms. Recommendations of the IUGS Subcommission on the Systematics of Igneous rocks. Blackwell, Oxford

Lowe DJ, Davies SM, Moriwaki H, Pearce NJG, Suzuki T (2011) Preface: enhancing tephrochronology and its application (INTREPID project): Hiroshi Machida commemorative volume. Quatern Int 246:1–5 (**Elsevier**)

Lowe DJ, Pearce NJG, Jorgensen MA, Kuehn SC, Tryon CA, Hayward CL (2017) Correlating tephras and cryptotephras using glass compositional analyses and numerical and statistical methods: review and evaluation. Quatern Sci Rev 175:1–44 (**Elsevier**)

Malaguti AB, Branca S, Speranza F, Coltelli M, Del Carlo P, Renzulli A (2023) Age of the Valle del Bove formation and chronology of the post-collapse flank eruptions, Etna volcano (Italy). J Volcanol Geotherm Res 434:107752 (**Elsevier**)

Menke V, Kutterolf S, Sievers C, Schindlbeck JC, Schmiedl G (2018) Cryptotephra from Lipari Volcano in the eastern Gulf of Taranto (Italy) as a time marker for paleoclimatic studies. Quatern Res 89:520–532 (**Cambridge University Press**)

Micallef A, Georgiopoulou A, Mountjoy J, Huvenne VAI, Iacono CL, Le Bas T, Del Carlo P, Otero DC (2016) Outer shelf seafloor geomorphology along a carbonate escarpment: the eastern Malta Plateau, Mediterranean Sea. Edited by Elsevier. Cont Shelf Res 131:12–27

Mulas M, Cioni R, Andronico D, Mundula F (2016) The explosive activity of the 1669 Monti Rossi eruption at Mt. Etna (Italy). J Volcanol Geotherm Res 328:115–133 (**Elsevier**)

Pierre S, Clocchiatti R, Ottolini L, Sbrana A (2004) The relationship between potassic, calc-alkaline and Na-alkaline magmatism in South Italy volcanoes: a melt inclusion approach. Earth Planet Sci Lett 220(Issues 1–2):121–137, ISSN 0012–821X. https://doi.org/10.1016/S0012-21X(04)00048. (https://www.sciencedirect.com/science/article/pii/S0012821X04000482)

Pearce NJG, Bendall CA, Westgate JA (2008) Comment on "Some numerical considerations in the geochemical analysis of distal microtephra" by AM Pollard, SPE Blockley and CS Lane. Appl Geochem 5:1353–1364

Pearce NJG, Westgate JA, Gatti E, Pattan JN, Parthiban G, Achyuthan H (2014a) Individual glass shard trace element analyses confirm that all known Toba tephra reported from India is from the c. 75-ka Youngest Toba eruption. J Quatern Sci 29:729–734 (**Wiley Online Library**)

Pearce NJG, Abbott PM, Martin-Jones C (2014b) "Microbeam methods for the analysis of glass in fine-grained tephra deposits: a SMART perspective on current and future trends. Geol Soc Lond Spec Publ 398:29–46 (**Geological Society of London**)

Reimer PJ, Austin WE, Bard E, Bayliss A, Blackwell PG, Ramsey CB et al (2020) The IntCal20 Northern Hemisphere radiocarbon age calibration curve (0–55 cal kBP). Radiocarbon 62(4):725–757

Romano R (1982) Succession of the volcanic activity in the Etnean area. Mem Soc Geol Ital 23:27–48

Rossignol-Strick M (1985) Mediterranean Quaternary sapropels, an immediate response of the African monsoon to variation of insolation. Palaeogeogr Palaeoclimatol Palaeoecol 49:237–263

Sadori L, Narcisi B (2001) The Postglacial record of environmental history from Lago di Pergusa, Sicily. The Holocene 11:655–671 (**Sage Publications Sage CA: Thousand Oaks, CA**)

Salvi F, Scandone R, Palma C (2006) Statistical analysis of the historical activity of Mount Etna, aimed at the evaluation of volcanic hazard. J Volcanol Geotherm Res 154:159–168 (**Elsevier**)

Schindlbeck JC, Kutterolf S, Freundt A, Scudder RP, Pickering KT, Murray RW (2013) Emplacement processes of submarine volcaniclastic deposits (IODP Site C0011, Nankai Trough). Mar Geol 343:115–124 (**Elsevier**)

Schindlbeck JC, Kutterolf S, Armin Freundt GE, Alvarado K-L, Wang SM, Straub SR, Hemming MF, Woodhead JD (2016) "Late C enozoic tephrostratigraphy offshore the southern C entral A merican V olcanic A rc: 1. Tephra ages and provenance. Geochem Geophys Geosyst 17:4641–4668 (**Wiley Online Library**)

Schindlbeck JC, Kutterolf S, Freundt A, Eisele S, Wang K-L, Frische M (2018a) Miocene to Holocene marine tephrostratigraphy offshore northern Central America and southern Mexico: pulsed activity of known volcanic complexes. Geochem Geophys Geosyst 19:4143–4173 (**Wiley Online Library**)

Schindlbeck JC, Kutterolf S, Straub SM, Andrews GDM, Wang K-L, Mleneck-Vautravers MJ (2018b) One million years tephra record at IODP Sites U 1436 and U 1437: insights into explosive volcanism from the Japan and Izu arcs. Island Arc 27:e12244 (**Wiley Online Library**)

Simkin T, Siebert L (2005) Global Volcanism Program: worldwide Holocene volcano and eruption information (www. volcano. si. edu.). Smithsonian Institution, Washington DC

Sulpizio R, Van Welden A, Caron B, Zanchetta G (2010) The Holocene tephrostratigraphic record of Lake Shkodra (Albania and Montenegro). J Quat Sci 25:633–650. https://doi.org/10.1002/jqs.1334

Tomlinson EL, Smith VC, Albert PG, Aydar E, Civetta L, Cioni R, Çubukçu E et al (2015) The major and trace element glass compositions of the productive Mediterranean volcanic sources: tools for correlating distal tephra layers in and around Europe. Quatern Sci Rev 118:48–66 (**Elsevier**)

Vogel H, Zanchetta G, Sulpizio R, Wagner B, Nowaczyk N (2010) A tephrostratigraphic record for the last glacial–interglacial cycle from Lake Ohrid, Albania and Macedonia. Journal of Quaternary Science: Published for the Quaternary Research Association 25(3):320–338

Wagner B, Sulpizio ROBERTO, Zanchetta G, Wulf S, Wessels M, Daut G, Nowaczyk N (2008) The last 40 ka tephrostratigraphic record of Lake Ohrid, Albania and Macedonia: a very distal archive for ash dispersal from Italian volcanoes. J Volcanol Geotherm Res 177(1):71–80